Journal of Materials Chemistry A

Accepted Manuscript

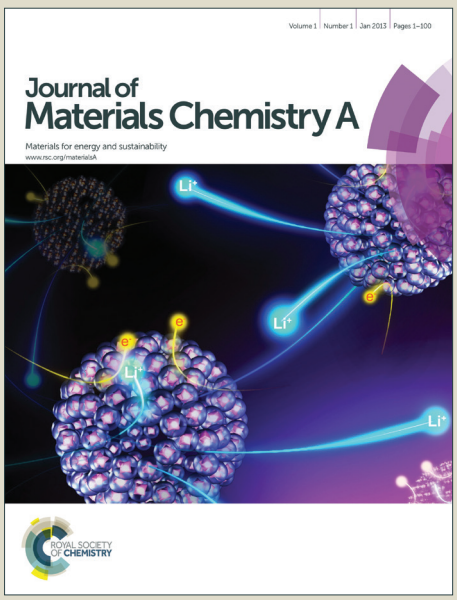

ROYAL SOCIETY OF CHEMISTRY

www.rsc.org/materialsA

Morphology-Controlled $CH_3NH_3PbI_3$ Films by Hexane-Assisted One-Step Solution Deposition for Hybrid Perovskite Mesoscopic Solar Cells with High Reproductivity

Na Lin, Juan Qiao*, Haopeng Dong, Fusheng Ma, Liduo Wang

Key Lab of Organic Optoelectronics and Molecular Engineering of Ministry of Education, Department of Chemistry, Tsinghua University, Beijing 100084, P. R. China
Corresponding author: * Email: qjuan@mail.tsinghua.edu.cn; Fax: +86-10-62795137

Table of contents entry:

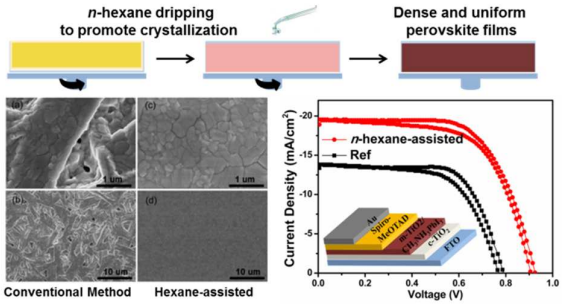

Morphology-controlled and uniform perovskite films were realized by using *n*-hexane to promote the crystallization of $CH_3NH_3PbI_3$, thus improving the thermal stability of $CH_3NH_3PbI_3$ and performance of the corresponding perovskite solar cells.

Abstract

The morphology and crystal structure of perovskite films is critical for achieving high-performance perovskite solar cells, however in most cases, the conventional one-step solution deposition method hardly yield a homogeneous perovskite film over a large area, especially for $CH_3NH_3PbI_3$. Here we propose a facile and environment-friendly hexane-assisted one-step solution approach for dense and uniform $CH_3NH_3PbI_3$ thin films. According to the phase diagram of immiscible liquids, *n*-hexane was chosen as the assistant solvent to speed-up the evaporation of the main solvent *N,N*-dimethylformamide (DMF) during solution deposition process, thus significantly promote the nucleation

and crystallization process of $CH_3NH_3PbI_3$ perovskite. The as-prepared $CH_3NH_3PbI_3$ films demonstrated uniform and dense morphology, and enhanced light absorption in long-wavelength range. In particular, such *n*-hexane treatment could help eliminate the residue DMF and greatly improve the thermal stability of the obtained perovskite films. The full solution-processed $CH_3NH_3PbI_3$ solar cells using *n*-hexane treatment exhibited a maximum power conversion efficiency of 11.7% and average efficiencies of 11.3±0.4% under standard AM 1.5 conditions in comparison with 7.0±0.4% of the conventional cells. The recombination resistance of the cells increased nearly 5 times by using *n*-hexane. These results suggest that this hexane-assisted one-step solution approach is promising for controlling the crystallization process of $CH_3NH_3PbI_3$ to achieve high-performance perovskite solar cell.

1. Introduction

Lead organohalide perovskite $CH_3NH_3PbI_3$ and its mixed-halide derivatives have attracted tremendously growing attention in photovoltaic field during the past five years[1–6] due to their superior physical properties such as strong light harvesting capability,[7,8] tunable bandgaps,[9] long electron and hole diffusion lengths,[10] and ambipolar charge transport.[11] With the great research efforts contributed, the power conversion efficiency (PCE) of these perovskite solar cells have increased from 4%[7] up to 20 %,[12,13] which is much higher than other third-generation thin film solar cells.[1–6] In addition to their excellent photovoltaic performance, perovskite solar cells also possess solution-processable property, which could lower the fabrication cost and promote their wide commercialization in the future.

Controlling the morphology and crystal structure of perovskite film is critical for developing high-performance solar cells.[14–16] Until now, there are two solution deposition methods to prepare perovskite films, take $CH_3NH_3PbI_3$ as the example: (1) one-step solution deposition directly from a lead-halide perovskite precursor solution,[7,8] and (2)

sequential deposition of solution processed PbI_2 followed by a solution or gas phase exposure to CH_3NH_3I.[11,17] Compared to the two-step sequential solution deposition, one-step solution deposition is both advantageous and timesaving. However, in most cases, the conventional one-step solution deposition method hardly yield a homogeneous perovskite film over a larger area, especially for $CH_3NH_3PbI_3$.[18–20]

To date, much efforts have been devoted to control the crystallization of perovskite during the one-step solution deposition,[18] such as adjusting the concentration and solvent of the precursor solutions,[21] using additive to the precursor[22] as well as annealing control.[23] For instance, Zhu *et. al* found that adding CH_3NH_3Cl to the standard perovskite precursor can affect the crystallization process, thus leading to significantly improved coverage of $CH_3NH_3PbI_3$ film on a planar substrate.[22] Cheng and Spiccia *et. al* reported a uniform and dense perovskite layer by dripping another solvent such as chlorobenzene during a one-step solution deposition.[24] These methods could promote the crystallization of perovskites and result in good morphology and dense film, but involve high boiling point solvents (eg. chlorobenzene[24] and toluene[25]) or require a relative long time for annealing (eg. using CH_3NH_3Cl[22] or 1,8-diiodooctane as additive[15,26]).

In this work, we attempted to develop a facile and environment-friendly hexane-assisted one-step solution approach to achieve dense and uniform perovskite films. Unlike toluene and chlorobenzene which is miscible with main solvent such as *N,N*-dimethylformamide (DMF) and would involve with the perovskite precursor, *n*-hexane is immiscible with DMF and has relatively low boiling point, high vapor pressure and low toxicity. According to the phase diagram of immiscible liquids, when *n*-hexane as the assistant solvent is introduced during the spinning-coating of perovskite precursor, the evaporation rate of the main solvent DMF would be greatly accelerated due to the highly increased total vapor pressure, thus helping promote the nucleation, growth and uniform solid

perovskite formation. By dripping *n*-hexane to the substrate during deposition process, we obtained dense and highly uniform $CH_3NH_3PbI_3$ films with enhanced light harvesting in long-wavelength range. Most notably, the residue DMF in the perovskite film could be eliminated by the *n*-hexane treatment and the as-prepared perovskite films have higher thermal stability than the conventional one. Compared to the conventional one-step solution approach, using *n*-hexane significantly improved the performance of mesoscopic $CH_3NH_3PbI_3$ solar cells from 7.0±0.4% to 11.3±0.4% under standard AM 1.5 conditions. In addition, we anticipate this work would deepen the understanding on the formation mechanism of the perovskite films.

2. Results and discussion

In the conventional one-step deposition process, the formation of the perovskite layer is realized by spin-coating the precursor solution on the substrate followed by thermal annealing to complete the perovskite formation from the precursors. This deposition process usually consists of two stages. In the initial stage, the excess solution is spun off due to the centrifugal forces leading to the liquid film thinning. After a transition point, film thinning dominated by evaporation of solvent, which depends on the vapor pressure of the solvent.[27,28] Then the solution becomes supersaturated, nucleation, growth and solid perovskite (or intermediate) film forms. If we assume the $CH_3NH_3PbI_3$ solution as the ideal (Newtonian) liquid and the evaporation rate is constant, the amount of materials deposited at the end of the spinning process in the dry film (Γ) can be written as:[27,28]

$$\Gamma \approx c_0 \left(\frac{E}{3\nu}\right)^{\frac{1}{3}} \omega^{-\frac{2}{3}} \qquad (1)$$

Where c_0 and ν is the concentration and viscosity of solution respectively, ω is the spinning speed, and E is the evaporation rate. In most cases, DMF is used as a polar solvent to dissolve the perovskite precursor, which has very low vapor pressure (0.52 kPa at 20 ^{o}C) and very high boiling point (154 ^{o}C under 1 atm). Consequently, the evaporation of DMF and crystal nucleation rate of the perovskite material is very slow in the conventional one-step

solution deposition process, thus leading to large elongated perovskite crystal plates and/or submicrometer-sized islands with many inevitable uncovered pin-hole areas in the resulted perovskite films.[11,24]

To prepare uniform, pinhole-free perovskite $CH_3NH_3PbI_3$ films by conventional solution deposition, the key point is how to improve the evaporation rate of DMF and control the crystallization process of perovskite. In principle, for two immiscible liquids, the total vapor pressure of the mixture is close to $\boldsymbol{p} = \boldsymbol{p}_{\mathbf{A}}^{*} + \boldsymbol{p}_{\mathbf{B}}^{*}$, consequently the boiling point of the mixture would be lower than either component.[29] Inspired by this principle, we consider that if a second solvent, which has very high vapor pressure but is immiscible with DMF, is introduced during the spinning-coating of perovskite precursor, the evaporation rate of DMF would be greatly accelerated, thus helping promote the nucleation, growth and uniform solid perovskite formation.

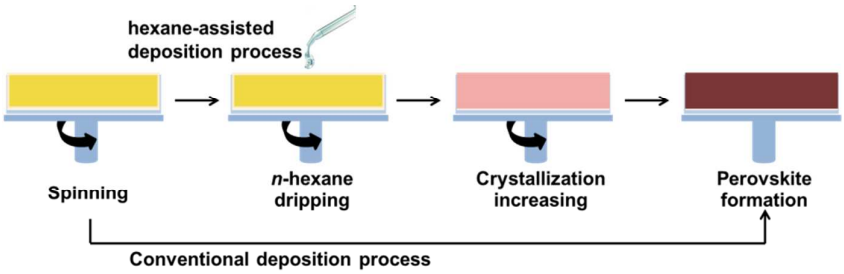

Figure 1. Schematic illustration of the conventional and *n*-hexane-assisted one-step solution deposition process to form perovskite $CH_3NH_3PbI_3$ film.

Given the miscibility of the common solvents, only *n*-hexane, *n*-heptane and *cyclo*-hexane are immiscible with DMF. Among them, *n*-hexane is the best candidate because of its significantly higher vapor pressure (13.3 kPa at 25 ^{o}C), lower boiling point (68 ^{o}C under 1 atm) and lower toxicity than the other two. Figure 1 depicts the scheme of the *n*-hexane-assisted one-step solution deposition process compared with the conventional process to form perovskite

$CH_3NH_3PbI_3$ films. At first, a DMF solution of $CH_3NH_3PbI_3$ precursor solution was spin-coated on the compact TiO_2 (c-TiO_2) layer. After a specific delay time (around 8~10s), *n*-hexane was quickly dripped to the substrate and immediately a brown film formed, which is presumably caused by great increase of the total vapor pressure leading to fast crystallization of the perovskite $CH_3NH_3PbI_3$.

Figure 2 shows the typical scanning electron microscopy (SEM) images of top views of the annealed perovskite films from the conventional and *n*-hexane-assisted one-step deposition procedure, respectively. When no *n*-hexane is used, the perovskite film is composed of large, needle-shape crystals with micrometer-sized uncovered areas (Figure 2 (a) and (b)). When *n*-hexane is added at around 8~10 s, large elongated crystal plates totally disappear and the film is full of interconnected micrometer-sized grains with full surface coverage on the substrate (Figure 2 (c) and (d)). In addition, for the perovskite $CH_3NH_3PbI_3$ films on the mesoporous-TiO_2 (m-TiO_2) layer, dripping *n*-hexane could also help form uniform and dense perovskite layers (Figure S1). That demonstrated that dripping *n*-hexane during perovskite deposition process could promote the crystal nucleation and growth process and result in good morphology and dense films. To be noted, if we dripped *n*-hexane too early (e.g. around 6~8 s) when the perovskite solution is far from supersaturation or too later (e.g. around 12~14 s) when the perovskites have started crystallizing, the uniform perovskite film did not form (see Figure S2).

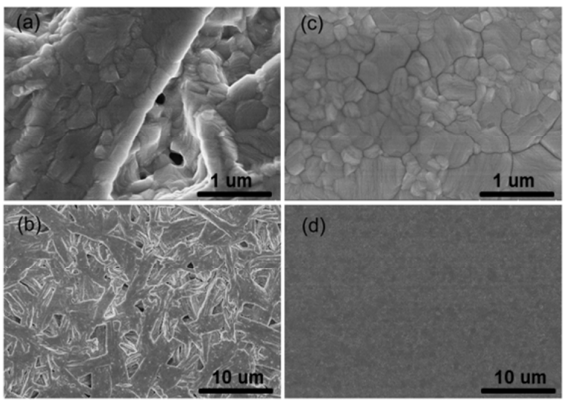

Figure 2. Typical SEM images of perovskite $CH_3NH_3PbI_3$ grown on c-TiO_2 layer by conventional (a-b) and hexane-assisted (c-d) one-step solution deposition method.

The X-ray diffraction (XRD) patterns of these two $CH_3NH_3PbI_3$ films were compared in Figure 3(a). Both perovskite $CH_3NH_3PbI_3$ films show very similar strong Bragg peaks at 14.21 ^{o}(110), 28.49 ^{o}(220), 31.95 ^{o}(310) and 43.25 ^{o}(330), which correspond to a tetragonal I_4cm crystal structure of $CH_3NH_3PbI_3$.[5] It is interesting to note that the relative intensities of the peaks at 28.49 and 31.95 are different between these two films. This may suggest a slight change of the preferred orientation of perovskites with the *n*-hexane addition during the deposition process. Besides, the full width at half maximum (FWHM) at (110) reflection of these two films are almost the same (Figure S3), indicating the similarity in the X-ray crystallite size. This means that both perovskite films have almost the same the crystallinity.[25] Most notably, these two perovskite films exhibit the same optical energy gap but large disparity in the long-wavelength light absorbance. As shown in Figure 3(b), the *n*-hexane-assisted film shows significantly increased light harvesting in the long wavelength regime, which could attributed to the full film coverage and uniform morphology.

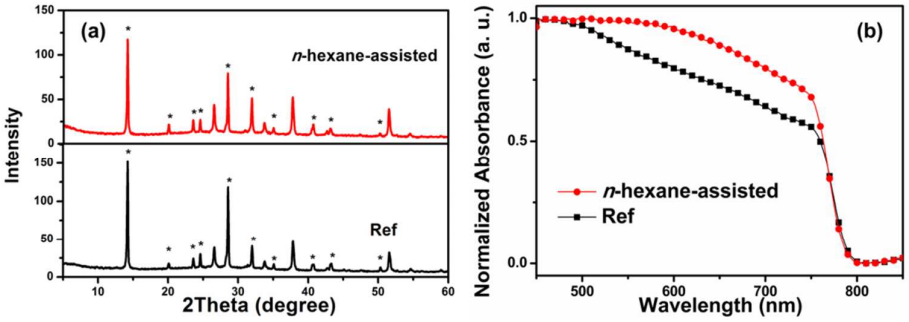

Figure 3. XRD patterns (a) and normalized absorbance spectra (b) of the $CH_3NH_3PbI_3$ perovskite films prepared by conventional and hexane-assisted one-step solution deposition. The XRD peaks assigned to $CH_3NH_3PbI_3$ crystals are marked with asterisks.

The thermal stability of these perovskite samples was investigated by means of differential scanning calorimetry (DSC) measurements. Figure 4 shows the DSC curves of the perovskite samples scratched from the solution-deposited films. For the perovskite sample from the conventional solution process, there are clear transition peaks at 56 and 54 ^{o}C during the first heating and cooling processes respectively, which correspond to the phase transition from tetragonal to cubic of $CH_3NH_3PbI_3$. It is worth to note that there are additional small but clearly visible endothermic peaks around 89 and 148 ^{o}C during the first heating process, which are absent in the first cooling and the subsequent second heating processes. These transitions could be tentatively ascribed to the removal of the absorbed H_2O and residual DMF in the film. This indicates that there is still a small amount of DMF remained in the $CH_3NH_3PbI_3$ film deposited from conventional deposition process even after thermal annealing, which might exist as the intermediate phase such as $CH_3NH_3PbI_3$•DMF or PbI_2•DMF.[12,30,31] In comparison, in the case of perovskite sample from the *n*-hexane-assisted solution process, none of the above transition peaks appear in the first heating process, while the typical phase transition peak around 56 ^{o}C comes out during the first cooling and the second heating process (Figure 4b). This suggests the perovskite film from the *n*-hexane-assisted solution process has very different thermal history and microstructures from the conventional solution process. The absence of the transition at 89 and 148 ^{o}C indicates that the use of *n*-hexane helps to eliminate the solvent DMF. Although immiscible with DMF, *n*-hexane has very high vapor pressure and its addition can quickly increase the total vapor pressure of the precursor mixture, thus significantly promote the evaporation of DMF and speed-up the crystallization of the perovskite. The absence of the transition peak at 56 ^{o}C during the first heating process just demonstrates that difference in the obtained perovskite films.

Furthermore, we comparatively studied the thermal degradation behavior of these perovskite films after heating at 85

°C in the N_2 glove box for 24 h. As shown in Figure 4c, After 24 h heating at 85 °C, both films demonstrate a new peak at 12.69 ° in the XRD patterns, which could be ascribed to the PbI_2 (001) plane due to the thermal dissociation of perovskites.[32] However, for the *n*-hexane-assisted film, this peak is relatively smaller, suggesting that such thermal degradation is reduced to some extent. That could be attributed to the removal of the residual DMF by the *n*-hexane treatment. It is reported that polar DMF solvent can coordinate with PbI_2 and form some intermediate phase during the crystallization process of perovskites.[31] Accordingly, the residual DMF in the thermal-annealed films could likewise form coordination with PbI_2 and then the unbound CH_3NH_3I could readily escape the structure and leave behind PbI_2. Thus, the remained DMF even in trace in conventional film would accelerate chemical thermal degradation of $CH_3NH_3PbI_3$.

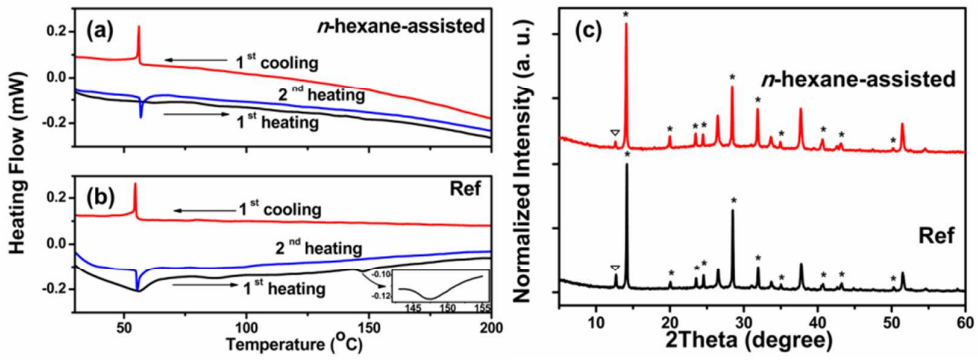

Figure 4. DSC curves for the $CH_3NH_3PbI_3$ samples scratched off the films prepared from the hexane-assisted (a) and conventional process (b) under a dry nitrogen gas flow at a heating rate of 10 °C min^{-1}. (c) XRD patterns of thermal aged $CH_3NH_3PbI_3$ films at 85 °C in the N_2 glove box for 24 hr.

The effects of hexane-assisted treatment were investigated via mesoporous perovskite solar cells. The mesoporous devices have the structure of FTO/c-TiO_2/m-TiO_2/$CH_3NH_3PbI_3$/Spiro-OMeTAD/Au (shown in Figure 5a), where the Spiro-OMeTAD is 2,2',7,7'-tetrakis[*N,N*-di(4-methoxyphenyl)amino]-9,9'-spirobifluorene and used as the

hole-transporting layer, and the perovskite layers were deposited by conventional or hexane-assisted one-step solution deposition. The devices performance data are shown in Figure 5a and summarized in Table 1. The current-voltage (*J*-*V*) curves of these solar cells were measured with a 500 ms scanning delay in reverse (from the open-circuit voltage (V_{oc}) to the short-current density (J_{sc})) and forward (from J_{sc} to V_{oc}) modes under standard global AM 1.5 illumination.

As depicted in Figure 5a, the reference devices in which the perovskite layer was fabricated with the conventional one-step solution method show a J_{sc} of 13.8 mA/cm^2, a V_{oc} of 0.79 V, fill factor (*FF*) of 68 %, and a total PCE of 7.4% obtained from the reverse scan. While the devices in which the perovskite layers were treated with *n*-hexane show significant enhancement in the photovoltaic parameters. The best-performing devices demonstrate a J_{sc} of 19.5 mA/cm^2, a V_{oc} of 0.93 V, and *FF* of 65 %, corresponding to an overall PCE of 11.7% obtained from the reverse scan. The average PCE tested by fabricating 20 devices (Figure S4 and Table 1) of the devices with hexane-assisted films is 11.3±0.4%, which is also much higher than that of the conventional solution-deposited one with 7.0±0.4%. This indicates that *n*-hexane-assisted solution process could greatly improve the device performance and reproducibility. Consequently, the incident photon-to-electron conversion efficiency (IPCE) (Figure S5) of the devices prepared by *n*-hexane-assisted process exhibit significant improvement in the range of 400-750 nm compared to the conventional ones. To rule out the influence of hysteresis effects, we performed the photocurrent density and power conversion efficiency as a function of time for these cells held at a forward bias of 0.62 and 0.56 V respectively. The photocurrent density of the devices prepared by *n*-hexane-assisted stabilizes within 240 s and a highly stable power output of 10.3 % could be obtained, which is also much higher than that of conventional one (5.4 %) (Figure S6). Besides, we also studied the effects of hexane-assisted treatment in the planar devices with the structure of FTO/c-TiO_2/$CH_3NH_3PbI_3$/Spiro-OMeTAD/Au. Likewise, the devices with *n*-hexane treatment demonstrate

significantly improved performance in terms of J_{sc}, V_{oc} and PCE compared to the conventional ones (Figure S7).

The improvement in the cell performance mainly lies in the increase of J_{sc} and V_{oc} compared to the reference devices. First, the enhancement of J_{sc} can be well explained with greatly improved light absorption caused by the improved perovskite morphology. The higher coverage and condense perovskite film obtained from the *n*-hexane treatment have higher light-harvest capability than the reference film (Figure 3b), thus increasing the current generated. Meanwhile, the improvement of V_{oc} can be attributed to retarding the recombination in the hexane-treatment devices. V_{oc} can be determined using the formula as:

$$V_{oc} = \left(\frac{mRT}{F}\right)\ln\left(\frac{I_{sc}}{I_0} - 1\right)^{32} \quad (2)$$

where I_{sc} is the short-circuit photocurrent, I_0 is the dark current, m is the ideality factor, whose value is between 1 and 2 for perovskite solar cells, and R and F are the ideal gas and Faraday constants, respectively. According to the formula (2), V_{oc} increases with I_0 decreasing. We measured the dark current of the two devices. The devices with perovskite films obtained from *n*-hexane treatment showed much higher dark current onset than the devices obtained from the conventional process (Figure S8). It suggests that the charge recombination in the former devices were effectively suppressed. In addition, we also performed the electrochemical impedance spectra (EIS) measurements to trace the charge-transfer process in these devices. Figure 4b shows the Nyquist plot of the devices measured in the dark at a forward bias of 0.6V. It is reported that the Middle-frequency semicircle in the Nyquist plots in such perovskite solar cells represents the charge transfer resistance related to the recombination of electrons in the TiO_2 with holes in perovskite or hole transport layer.[34,35] The values changed from 2136 Ohm of the reference devices to 12133 Ohm of the devices by hexane-treatment, which means the electrons and holes recombination was markedly restrained when the perovskite layer was treated with *n*-hexane.

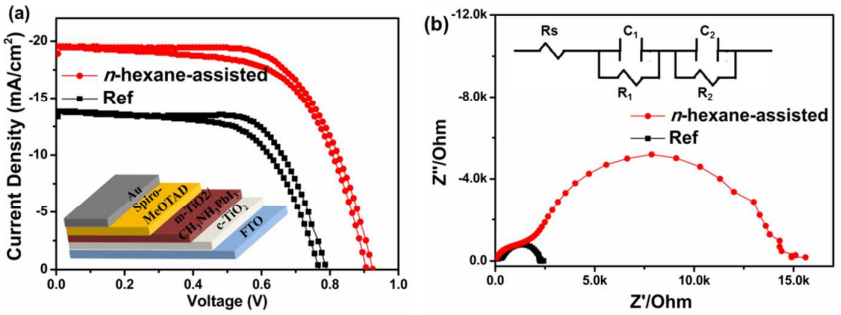

Figure 5. (a) The *J*–*V* characteristics of devices with and without hexane-assisted solution deposition process; the inset shows the device architecture of the depleted perovskite solar cell. (b) Nyquist plots under dark condition with 0.6 V bias voltage.

Table 1. Device parameters for the $CH_3NH_3PbI_3$-based devices from different deposition method. Average values are determined from 20 devices.

Cell	V_{oc} (V)	J_{sc} (mA/cm^2)	*FF*	PCE (%)
n-hexane-assisted	0.93±0.2	18.8±0.7	0.65±0.3	11.3±0.4
Ref.	0.81±0.2	12.7±1.1	0.68±0.3	7.0±0.4

To further figure out the charge transfer process in the perovskite film and TiO_2/$CH_3NH_3PbI_3$/spiro-OMeTAD interface, we performed the photoluminescence (PL) measurement of the films of glass/$CH_3NH_3PbI_3$, FTO/c-TiO_2/$CH_3NH_3PbI_3$ and glass/$CH_3NH_3PbI_3$/spiro-OMeTAD, respectively. As can be seen from Figure 6a, for the films of glass/$CH_3NH_3PbI_3$, the PL intensity increases significantly when the $CH_3NH_3PbI_3$ film was treated with *n*-hexane. The increased PL intensity could be related to the decreased traps density[36] due to its dense and uniform morphology. Compared to the films of glass/$CH_3NH_3PbI_3$ without TiO_2, the PL of FTO/c-TiO_2/$CH_3NH_3PbI_3$ films is generally reduced due to injection of electrons from perovskite to TiO_2. The relative reduction of PL is much more significant when the $CH_3NH_3PbI_3$ film was treated with *n*-hexane (Figure 6b), which indicates effective electron-injection from perovskite to TiO_2 due to the homogeneous surface.[36] Likewise, the film of

glass/$CH_3NH_3PbI_3$/spiro-OMeTAD with the *n*-hexane treatment showed marked relative reduction of PL, suggesting effective hole-injection of from perovskite to spiro-OMeTAD. Such effective electron and hole-injection could contribute to better charge collection, consequently resulting in higher V_{oc} and J_{sc}. This is well consistent with the above discussion.

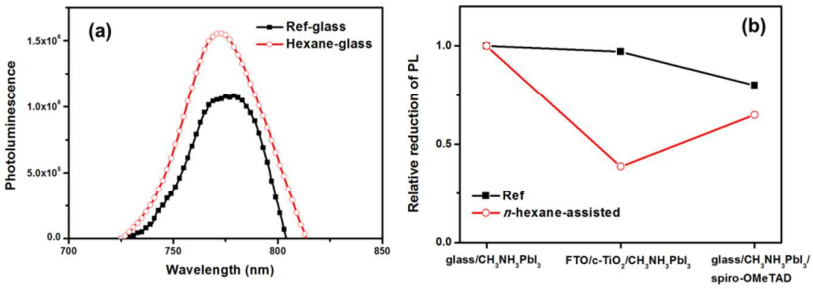

Figure 6. PL spectra of the glass/$CH_3NH_3PbI_3$ films (a); Relative PL reduction of FTO/c-TiO_2/$CH_3NH_3PbI_3$ and glass/$CH_3NH_3PbI_3$/spiro-OMeTAD films compared to glass/$CH_3NH_3PbI_3$ (b), where the $CH_3NH_3PbI_3$ films are treated with and without n-hexane, respectively.

In addition, we carried out a preliminary stability investigation of the perovskite solar cell without encapsulation by storing the devices under ambient conditions with controlled humidity about 50%. The conventional devices without *n*-hexane treatment show a rapid deterioration with PCE dropping to 5% after 240 hours as depicted in Figure S9. In comparison, the *n*-hexane-assisted devices exhibit a much slower deterioration with the PCE maintaining over 40% after 240 hours, suggesting less sensitivity to humidity, which could be correlated with its improved stability of the perovskite film.

3. Conclusion

In summary, we have developed a novel solvent-assisted one-step solution deposition method to prepare a uniform

$CH_3NH_3PbI_3$ films by dripping *n*-hexane during the spin-coasting process. The use of *n*-hexane could strongly promote the nucleation and crystal grain growth of $CH_3NH_3PbI_3$ perovskite by increasing the solvent evaporate rate, thus significantly improving the coverage of $CH_3NH_3PbI_3$ but also enhancing the absorption of $CH_3NH_3PbI_3$. In particular, our *n*-hexane-assisted method could help eliminate the residual DMF thus markedly improve the thermal stability of $CH_3NH_3PbI_3$ perovskite film. Taking advantage of these high-quality pinhole-free perovskite films, efficient hybrid perovskite solar cells on mesoporous TiO_2 demonstrated an average PCE of 11.3±0.4% and a steady state efficiency of 11.7% in comparison with 7.0±0.4% of the cells from the conventional method. These results demonstrate that this hexane-assisted one-step solution approach is promising for controlling the crystallization process of $CH_3NH_3PbI_3$ to achieve high-performance perovskite solar cell. Although this study focused on $CH_3NH_3PbI_3$ photovoltaic devices, we envisage that this approach would benefit other perovskite-based hybrid optoelectronic devices.

4. Experimental

Materials. PbI_2 was purchased from Alfar Aesar, CH_3NH_3I from Xi'an Polymer Light Technology Corp., DMF, chlorobenzene, lithium bis(trifluoromethylsulphonyl)imide (Li-TFSI) and 4-tert-butylpyridine (*t*BP) from Aldrich, and spiro-MeOTAD from Luminescence Technology Corp., Taiwan. All chemicals were directly used without further purification. Patterned FTO coated glass substrates with a sheet resistance of 12 Ω/square were cleaned sequentially by ultrasonication in mild detergent, deionized water, acetone, ethanolamine and isopropanol. The substrates were exposed to UV-ozone for 20 min prior to the spin coating step.

Perovskite photovoltaic cells fabrication. A dense TiO_2 layers were spin-coated on the FTO glass and calcined at 450 ^oC for 30 min. The nanocrystalline TiO_2 paste (18NRT from Dyesol Company, diluted to w/w 28.5%) was

deposited on the pretreated FTO substrate at 7000 rpm for 30 s, followed by heating at 500 ^{o}C for 1h. The CH_3NH_3I was mixed with PbI_2 at a 1:1 mol ratio in anhydrous DMF and stirred at 70 ^{o}C overnight to produce a $CH_3NH_3PbI_3$ solution with concentration of 40 wt%. For the conventional one-step solution deposition, the $CH_3NH_3PbI_3$/DMF solution was spin-coated onto the m-TiO2/c-TiO_2/FTO substrate at 2500 r.p.m. for 60 s. For the hexane-assisted one-step solution deposition, the substrate was spun at 2500 rpm and after 8-10 seconds anhydrous *n*-hexane was quickly dropped onto the substrate. Then the films were dried on a hot plate at 100 ^{o}C for 10 min. For the hole-transporting layer, a Spiro-MeoTAD/chlorobenzene (180 mg/ml) solution was used with added, 17.5 L Li-TFSI/acetonitrile solution (520 mg ml^{-1}) and 37.5 ul *t*BP. The $CH_3NH_3PbI_3$-coated TiO_2 films were covered with the HTM solution using the spin-coating method at 4000 rpm for 30 s. For the counter electrode, a 60 nm thick Au was deposited by thermal evaporation. The active area was fixed at 0.09 cm^2.

Characterization. The optical diffuse reflectance spectra of $CH_3NH_3PbI_3$ perovskite films were measured at room temperature using a UV-VIS-NIR spectrophotometer (Hitachi U-3010) with an integrating sphere attachment operating in the 350–850 nm regions. Highly refined barium sulfate powder was used as a reflectance standard. The XRD spectra of films were obtained using a Smart LAB instruments with an X-ray tube (Cu Kα, λ= 1.54 Å). The surface morphologies of perovskite films were investigated using the SEM (Hitachi SU-8010) with an accelerating voltage of 5 kV. DSC was recorded with a thermal analysis instrument (DSC 2910 modulated calorimeter) at a heating rate of 10 °C min^{-1} under nitrogen. The perovskite power was scratched off the substrate and used directly for the thermal analysis. The photocurrent-voltage (*J-V*) curves were measured under AM 1.5 irradiation (100 mW cm^{-2}, calibrated using an NREL-certified Si-reference cell) using a sun simulator (Oriel Solar Simulator 2000). The *J-V* character, IPCE and electrochemical impedance spectra (EIS, ranged from 0.1 Hz to 10^5 Hz) were measured by using a ZAHNER CIMPS electro-chemical workstation, Germany.

Acknowledgements

This work was supported by the National Nature Science Foundation of China (Grants No. 91233118 and 91433205) and the National Key Basic Research and Development Program of China under Grant No. 2011CB808403.

Notes and references

1 T. Song, Q. Chen, H.-P. Zhou, C. Jiang, H.-H. Wang, Y. Yang, Y. Liu, J. You and Y. Yang, *J. Mater. Chem. A*, 2015, **3**, 9032–9050.

2 S. D. Stranks and H. J. Snaith, *Nat. Nanotechnol.*, 2015, **10**, 391–402.

3 H. S. Jung and N.-G. Park, *Small*, 2015, **11**, 10–25.

4 S. Shi, Y. Li, X. Li and H. Wang, *Mater. Horiz.*, 2015, DOI: 10.1039/C4MH00236A.

5 T. Baikie, Y. Fang, J. M. Kadro, M. Schreyer, F. Wei, S. G. Mhaisalkar, M. Gratzel and T. J. White, *J. Mater. Chem. A*, 2013, **1**, 5628–5641.

6 P. Gao, M. Gratzel and M. K. Nazeeruddin, *Energy Environ. Sci.*, 2014, **7**, 2448–2463.

7 a Kojima, K. Teshima, Y. Shirai and T. Miyasaka, *J. Am. Chem. Soc.*, 2009, **131**, 6050–6051.

8 H.-S. Kim, C.-R. Lee, J.-H. Im, K.-B. Lee, T. Moehl, A. Marchioro, S.-J. Moon, R. Humphry-Baker, J.-H. Yum, J. E. Moser, M. Grätzel and N.-G. Park, *Sci. Rep.*, 2012, **2**, 1–7.

9 J. H. Noh, S. H. Im, J. H. Heo, T. N. Mandal and S. Il Seok, *Nano Lett.*, 2013, **13**, 1764–1769.

10 S. D. Stranks, G. E. Eperon, G. Grancini, C. Menelaou, M. J. P. Alcocer, T. Leijtens, L. M. Herz, A. Petrozza and H. J. Snaith, *Science*, 2013, **342**, 341–345.

11 J. Burschka, N. Pellet, S.-J. Moon, R. Humphry-Baker, P. Gao, M. K. Nazeeruddin and M. Grätzel, *Nature*, 2013, **499**, 316–319.

12 H. Zhou, Q. Chen, G. Li, S. Luo, T. -b. Song, H.-S. Duan, Z. Hong, J. You, Y. Liu and Y. Yang, *Science*, 2014, **345**, 542–546.

13 N. R. E. L. (NREL), http://www.nrel.gov/ncpv/images/efficiency_chart.jpg.

14 J.-H. Im, H.-S. Kim and N.-G. Park, *APL Mater.*, 2014, **2**, 081510(1)–(8).

15 P. W. Liang, C. Y. Liao, C. C. Chueh, F. Zuo, S. T. Williams, X. K. Xin, J. Lin and A. K. Y. Jen, *Adv. Mater.*, 2014, **26**, 3748–3754.

16 T. Salim, S. Sun, Y. Abe, A. Krishna, A. C. Grimsdale and Y. M. Lam, *J. Mater. Chem. A*, 2015, **3**, 8943–8969.

17 Q. Chen, H. Zhou, Z. Hong, S. Luo, H.-S. Duan, H.-H. Wang, Y. Liu, G. Li and Y. Yang, *J. Am. Chem. Soc.*, 2014, **136**, 622–625.

18 Y. Zhao and K. Zhu, *J. Phys. Chem. Lett.*, 2014, **5**, 4175–4186.

19 G. E. Eperon, V. M. Burlakov, P. Docampo, A. Goriely and H. J. Snaith, *Adv. Funct. Mater.*, 2014, **24**, 151–157.

20 H. S. Kim, S. H. Im and N. Park, *J. Phys. Chem. C*, 2014, **118**, 5615–5625.

21 J.-H. Im, C.-R. Lee, J.-W. Lee, S.-W. Park and N.-G. Park, *Nanoscale*, 2011, **3**, 4088–4093.

22 Y. Zhao and K. Zhu, *J. Phys. Chem. C*, 2014, **118**, 9412–9418.

23 A. Dualeh, N. Tétreault, T. Moehl, P. Gao, M. K. Nazeeruddin and M. Grätzel, *Adv. Funct. Mater.*, 2014, **24**, 3250–3258.

24 M. Xiao, F. Huang, W. Huang, Y. Dkhissi, Y. Zhu, J. Etheridge, A. Gray-Weale, U. Bach, Y. B. Cheng and L. Spiccia, *Angew. Chemie. Int. Ed.*, 2014, **3168**, 9898–9903.

25 N. J. Jeon, J. H. Noh, Y. C. Kim, W. S. Yang, S. Ryu and S. Il Seok, *Nat. Mater.*, 2014, **13**, 1–7.

26 C. Chueh, C. Liao, F. Zuo, S. T. Williams, P. Liang and A. K. Jen, *J. Mater. Chem. A*, 2015, **3**, 9058–9062.

27 D. T. W. Toolan, N. Pullan, M. J. Harvey, P. D. Topham and J. R. Howse, *Adv. Mater.*, 2013, **25**, 7033–7037.

28 Ghani, F. Nucleation and Growth of Unsubstituted Metal Phthalocyanine Films from Solution on Planar Substrates. Ph.D. Dissertation, Universitatsbibliothek Potsdam, Germany, 2013.

29 P. Atkins, J. de Paula, Atkins Physical Chemistry 7th Ed, Seventh Edition, Oxford University Press, 2005, 182-184.

30 F. Hao, C. C. Stoumpos, Z. Liu, R. P. H. Chang and M. G. Kanatzidis, *J. Am. Chem. Soc.*, 2014, **136**, 16411–16419.

31 D. Shen, X. Yu, X. Cai, M. Peng, Y. Ma, X. Su, L. Xiao and D. Zou, *J. Mater. Chem. A*, 2014, **2**, 20454–20461.

32 G. Niu, X. Guo and L. Wang, *J. Mater. Chem. A*, 2015, **3**, 8970–8980.

33 D. Gupta, S. Mukhopadhyay and K. S. Narayan, *Phys. Chem. Chem. Phys.*, 2013, **15**, 8972–8982.

34 X. Xu, H. Zhang, K. Cao, J. Cui, J. Lu, X. Zeng, Y. Shen and M. Wang, *Chem. Sus. Chem*, 2014, **7**, 3088–3094.

35 A. Dualeh, T. Moehl, N. Tétreault, J. Teuscher, P. Gao, M. K. Nazeeruddin and M. Grätzel, *ACS Nano*, 2014, **8**, 362–373.

36 D. Seol, J. Lee and N. Park, *Chem. Sus. Chem*, 2015, **8,** 2414–2419.